

Reconstructing Quasar Spectra and Measuring the Ly α Forest with SPENDERQ

CHANGHOON HAHN,^{1, 2, 3, *} SATYA GONTCHO A GONTCHO,^{4, 5} PETER MELCHIOR,²
 HIRAM K. HERRERA-ALCANTAR,^{6, 7} JESSICA NICOLE AGUILAR,⁸ STEVEN AHLEN,⁹
 DAVIDE BIANCHI,^{10, 11} DAVID BROOKS,¹² TODD CLAYBAUGH,⁸ AXEL DE LA MACORRA,¹³
 ARJUN DEY,¹⁴ PETER DOEL,¹² JAIME E. FORERO-ROMERO,^{15, 16} GASTON GUTIERREZ,¹⁷
 MUSTAPHA ISHAK,¹⁸ STEPHANIE JUNEAU,¹⁴ DAVID KIRKBY,¹⁹ THEODORE KISNER,⁸
 ANTHONY KREMIN,⁸ ANDREW LAMBERT,⁸ MARTIN LANDRIAU,⁸ LAURENT LE GUILLOU,²⁰
 MARC MANERA,^{21, 22} RAMON MIQUEL,^{23, 22} JOHN MOUSTAKAS,²⁴ ADAM D. MYERS,²⁵
 GUSTAVO NIZ,^{26, 27} NATHALIE PALANQUE-DELABROUILLE,^{6, 8} CLAIRE POPPETT,^{8, 28, 29}
 FRANCISCO PRADA,³⁰ IGNASI PÉREZ-RÀFOLS,³¹ GRAZIANO ROSSI,³² EUSEBIO SANCHEZ,³³
 DAVID SCHLEGEL,⁸ MICHAEL SCHUBNEL,^{34, 35} HEE-JONG SEO,³⁶ DAVID SPRAYBERRY,¹⁴
 GREGORY TARLÉ,³⁵ BENJAMIN A. WEAVER,¹⁴ AND HU ZOU³⁷

¹*Steward Observatory, University of Arizona, 933 N. Cherry Avenue, Tucson, AZ 85721, USA*

²*Department of Astrophysical Sciences, Princeton University, Princeton NJ 08544, USA*

³*Department of Astronomy, The University of Texas at Austin, 2515 Speedway, Stop C1400, Austin, TX 78712, USA*

⁴*Lawrence Berkeley National Laboratory, 1 Cyclotron Road, Berkeley, CA 94720*

⁵*University of Virginia, Department of Astronomy, Charlottesville, VA 22904, USA*

⁶*IRFU, CEA, Université Paris-Saclay, F-91191 Gif-sur-Yvette, France*

⁷*Institut d'Astrophysique de Paris. 98 bis boulevard Arago. 75014 Paris, France*

⁸*Lawrence Berkeley National Laboratory, 1 Cyclotron Road, Berkeley, CA 94720, USA*

⁹*Department of Physics, Boston University, 590 Commonwealth Avenue, Boston, MA 02215 USA*

¹⁰*Dipartimento di Fisica "Aldo Pontremoli", Università degli Studi di Milano, Via Celoria 16, I-20133 Milano, Italy*

¹¹*INAF-Osservatorio Astronomico di Brera, Via Brera 28, 20122 Milano, Italy*

¹²*Department of Physics & Astronomy, University College London, Gower Street, London, WC1E 6BT, UK*

¹³*Instituto de Física, Universidad Nacional Autónoma de México, Circuito de la Investigación Científica, Ciudad Universitaria, Cd. de México C. P. 04510, México*

¹⁴*NSF NOIRLab, 950 N. Cherry Ave., Tucson, AZ 85719, USA*

¹⁵*Departamento de Física, Universidad de los Andes, Cra. 1 No. 18A-10, Edificio Ip, CP 111711, Bogotá, Colombia*

¹⁶*Observatorio Astronómico, Universidad de los Andes, Cra. 1 No. 18A-10, Edificio H, CP 111711 Bogotá, Colombia*

¹⁷*Fermi National Accelerator Laboratory, PO Box 500, Batavia, IL 60510, USA*

¹⁸*Department of Physics, The University of Texas at Dallas, 800 W. Campbell Rd., Richardson, TX 75080, USA*

¹⁹*Department of Physics and Astronomy, University of California, Irvine, 92697, USA*

²⁰*Sorbonne Université, CNRS/IN2P3, Laboratoire de Physique Nucléaire et de Hautes Energies (LPNHE), FR-75005 Paris, France*

²¹*Departament de Física, Serra Hünter, Universitat Autònoma de Barcelona, 08193 Bellaterra (Barcelona), Spain*

²²*Institut de Física d'Altes Energies (IFAE), The Barcelona Institute of Science and Technology, Edifici Cn, Campus UAB, 08193, Bellaterra (Barcelona), Spain*

²³*Institució Catalana de Recerca i Estudis Avançats, Passeig de Lluís Companys, 23, 08010 Barcelona, Spain*

²⁴*Department of Physics and Astronomy, Siena College, 515 Loudon Road, Loudonville, NY 12211, USA*

²⁵*Department of Physics & Astronomy, University of Wyoming, 1000 E. University, Dept. 3905, Laramie, WY 82071, USA*

²⁶*Departamento de Física, DCI-Campus León, Universidad de Guanajuato, Loma del Bosque 103, León, Guanajuato C. P. 37150, México*

- ²⁷*Instituto Avanzado de Cosmología A. C., San Marcos 11 - Atenas 202. Magdalena Contreras. Ciudad de México C. P. 10720, México*
- ²⁸*Space Sciences Laboratory, University of California, Berkeley, 7 Gauss Way, Berkeley, CA 94720, USA*
- ²⁹*University of California, Berkeley, 110 Sproul Hall #5800 Berkeley, CA 94720, USA*
- ³⁰*Instituto de Astrofísica de Andalucía (CSIC), Glorieta de la Astronomía, s/n, E-18008 Granada, Spain*
- ³¹*Departament de Física, EEBE, Universitat Politècnica de Catalunya, c/Eduard Maristany 10, 08930 Barcelona, Spain*
- ³²*Department of Physics and Astronomy, Sejong University, 209 Neungdong-ro, Gwangjin-gu, Seoul 05006, Republic of Korea*
- ³³*CIEMAT, Avenida Complutense 40, E-28040 Madrid, Spain*
- ³⁴*Department of Physics, University of Michigan, 450 Church Street, Ann Arbor, MI 48109, USA*
- ³⁵*University of Michigan, 500 S. State Street, Ann Arbor, MI 48109, USA*
- ³⁶*Department of Physics & Astronomy, Ohio University, 139 University Terrace, Athens, OH 45701, USA*
- ³⁷*National Astronomical Observatories, Chinese Academy of Sciences, A20 Datun Road, Chaoyang District, Beijing, 100101, P. R. China*

ABSTRACT

Quasar spectra carry the imprint of foreground intergalactic medium (IGM) through absorption features. In particular, absorption caused by neutral hydrogen gas, the “Ly α forest,” is a key spectroscopic tracer for cosmological analyses used to measure cosmic expansion and test physics beyond the standard model. Despite their importance, current methods for measuring Ly α absorption cannot directly derive the intrinsic quasar continuum and make strong assumptions on its shape, thus distorting the measured Ly α clustering. We present SPENDERQ, a ML-based approach for directly reconstructing the intrinsic quasar spectra and measuring the Ly α forest from observations. SPENDERQ uses the SPENDER spectrum autoencoder to learn a compact and redshift-invariant latent encoding of quasar spectra, combined with an iterative procedure to identify and mask absorption regions. To demonstrate its performance, we apply SPENDERQ to 400,000 synthetic quasar spectra created to validate the Dark Energy Spectroscopic Instrument Year 1 Ly α cosmological analyses. SPENDERQ accurately reconstructs the true intrinsic quasar spectra, including the broad Ly β , Ly α , SiIV, CIV, and CIII emission lines. Redward of Ly α , SPENDERQ provides percent-level reconstructions of the true quasar spectra. Blueward of Ly α , SPENDERQ reconstructs the true spectra to $< 5\%$. SPENDERQ reproduces the shapes of individual quasar spectra more robustly than the current state-of-the-art. We, thus, expect it will significantly reduce biases in Ly α clustering measurements and enable studies of quasars and their physical properties. SPENDERQ also provides informative latent variable encodings that can be used to, e.g., classify quasars with Broad Absorption Lines. Overall, SPENDERQ provides a new data-driven approach for unbiased Ly α forest measurements in cosmological, quasar, and IGM studies.

* chhahn@arizona.edu

1. INTRODUCTION

Quasars or quasi-stellar objects (QSOs) are luminous active galactic nuclei fueled by gravitational accretion onto supermassive black holes at the centers of galaxies. As the most luminous extragalactic sources in the known universe, quasars are one of the main ways to study the cosmic large-scale structure in the early universe. Their spectra serve as cosmic lighthouses that probe the properties of the early universe through absorption from objects in their foreground. In particular, neutral hydrogen in the Inter-Galactic Medium (IGM) imprints a dense collection of absorption lines, blueward of the $\lambda = 1216\text{\AA}$ Ly α emission line, that make up the so-called “Ly α forest”.

As a tracer of neutral hydrogen, the Ly α forest traces the matter distribution and clustering in the Universe. On large cosmological scales, this enables us to use the three dimensional clustering of the Ly α forest to infer the expansion history of the Universe, using the Baryon Acoustic Oscillation feature as a “standard ruler” (e.g., [Busca et al. 2013](#); [Slosar et al. 2013](#); [Bautista et al. 2017](#); [du Mas des Bourboux et al. 2020](#)). They serve as an essential tracer over the redshift range $2 < z < 3$, where we currently do not have other reliable spectroscopic probes. Ly α absorption also continuously trace the matter distribution along the line of the sight of the background quasar on spatial scales as small as the spectral resolution. They serve as a unique probe of clustering on the smallest scales, down to few megaparsecs. This makes the Ly α forest one of the most promising tracers for precisely testing physics beyond the standard model: e.g., measuring neutrino mass (e.g., [Font-Ribera et al. 2014](#)) and probing the dark sector (e.g., [Bagherian et al. 2024](#); [Iršič et al. 2024](#)). Outside of cosmology, Ly α forests also enable us to probe properties of the IGM (temperature, density, and ionization state) in the early Universe ([Haardt & Madau 2012](#); [Madau & Haardt 2015](#); [Robertson et al. 2015](#); [Faucher-Giguère 2020](#)).

Given their broad cosmological and astrophysical applications, the Ly α forest has been one of the main tracers observed by recent spectroscopic galaxy surveys: e.g., the Baryon Oscillation Spectroscopic Survey (BOSS; [Eisenstein et al. 2011](#)) and the extended BOSS (eBOSS; [Ahumada et al. 2020](#)). The Dark Energy Spectroscopic Instrument (DESI; [Levi et al. 2013](#); [DESI Collaboration et al. 2016a,b, 2022](#)), the first Stage-IV galaxy survey, is continuing this effort on the 4m Mayall telescope at Kitt Peak National Observatory and with 5000 fiber positioners ([Guy et al. 2023](#); [Miller et al. 2024](#); [Silber et al. 2023](#); [Schlafly et al. 2023](#); [Poppett et al. 2024](#)). DESI has already more than quadruple the number of quasar spectra with Ly α from previous surveys, to roughly a million spectra.

To measure the Ly α forest and the full amplitude of its absorption, accurate knowledge of the original intrinsic quasar spectra (or continuum) is necessary. Yet, we only observe quasar spectra with Ly α absorption. As a result, the quasar continuum must be inferred from the absorbed spectra with only pieces of the unabsorbed spectra. This is only made more difficult by the higher neutral hydrogen fraction and density at higher redshifts. For some quasars, we observe little to none of their intrinsic spectra.

The current state-of-the-art, [picca](#)¹, entirely forgoes deriving the intrinsic quasar spectra, $C_q(\lambda)$. Instead, it derives the product $\overline{F}(\lambda)C_q(\lambda)$, i.e. the intrinsic spectrum multiplied by the mean trans-

¹ <https://github.com/igmhub/picca/>

mission fraction, which corresponds to the expected flux of the continuum. It further assumes that the product equates to a universal function in rest-frame, $G(\lambda/(1+z_q))$, and a polynomial with two free parameters (a_q, b_q) : $\bar{F}(\lambda)C_q(\lambda) = G(\lambda/(1+z_q))(a_q + b_q \log \lambda)$ (du Mas des Bourboux et al. 2020). This assumption does not reflect the range of continuum shapes in region “A” (the Ly α range from $\lambda/(1+z_q) = 1040$ to 1205\AA). `picca` also assumes that the flux transmission field, $\delta_q(\lambda) = f_q(\lambda)/(\bar{F}(\lambda)C_q(\lambda)) - 1$, has zero mean and slope. These assumptions distort the Ly α clustering measurements: e.g., they suppress the power spectrum by a factor of two on large scales with $k < 0.1 h^{-1}\text{Mpc}$ (Blomqvist et al. 2015; Karaçaylı et al. 2020, 2022, 2024; Ravoux et al. 2023; de Belsunce et al. 2024; Abdul Karim et al. 2024).

Many previous efforts have attempted to go beyond estimating $\bar{F}C_q$ and measure the unabsorbed continuum. For example, some works tried to exploit the correlation between the shape of the continuum on the red and blue side of Ly α to predict the continuum using principal component analysis (e.g., Suzuki et al. 2005; Pâris et al. 2011; Lee et al. 2012; Davies et al. 2018). More recent works have improved on this approach using ML. Liu & Bordoloi (2021) trained a neural network on Hubble Space Telescope/Cosmic Origin Spectrograph (COS) quasar spectra to predict the continuum in region A. Turner et al. (2024) used a similar approach with a convolutional neural network trained on a combination of COS spectra and DESI Year 5 mock spectra. While these supervised learning approaches show promising performance, they require training on labeled datasets and are, therefore, fundamentally limited by “data mismatch”. Any inaccuracies in the observationally derived ground truth or limitations in the simulations will degrade or bias their performance. Alternatively, Sun et al. (2023) recently used an unsupervised approach with Latent Factor Analysis to learn a model of the continuum. The model, however, makes assumptions on the shape of the continuum and requires modeling the Ly α forest, making it susceptible to any limitations in Ly α modeling.

We present SPENDERQ, a new method for reconstructing the intrinsic quasar spectra and measuring the Ly α forest that is fully data-driven and makes no assumptions on the shape of the continuum. SPENDERQ leverages the SPENDER autoencoder architecture (Melchior et al. 2023) to learn compact and redshift-invariant latent space representations of intrinsic quasar spectra. Since the foreground IGM are not correlated with the background quasars, SPENDER is especially well-suited for being insensitive to foregrounds and reconstructing the quasar continuum. SPENDERQ further combines SPENDER with an iterative procedure for identifying and masking Ly α absorption to further improve the fidelity of the reconstructions. It relaxes the current assumptions on the shape of the quasar continuum to produce unbiased Ly α forest measurements. Furthermore, as an entirely data-driven and unsupervised approach, SPENDERQ does not require any calibration on simulated data or labeled datasets. We start by applying SPENDERQ to synthetic Ly α data created to validate the DESI first year Ly α forest BAO analysis. Then, we compare our quasar reconstructions to the true quasar spectra to demonstrate its performance.

We begin by describing the SPENDERQ methodology for quasar spectra reconstruction (Section 2) and a brief description of the synthetic quasar spectra (Section 3). We then present and discuss our results in Section 4 and 5.

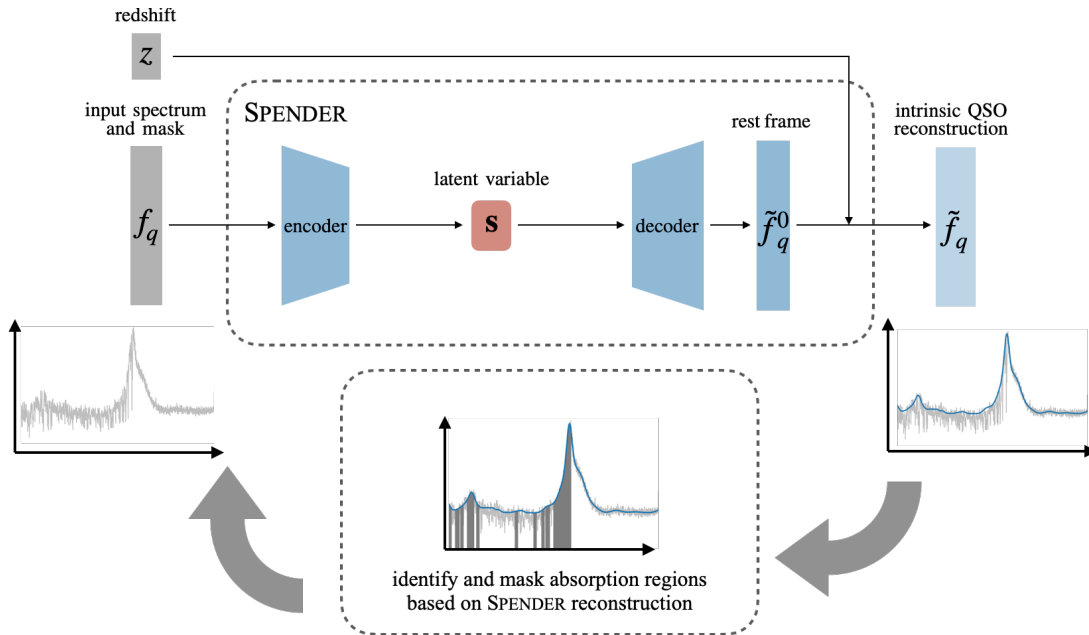


Figure 1. SPENDERQ combines the SPENDER autoencoder with an iterative procedure for masking absorption regions. It uses SPENDER to learn a compact and redshift-invariant latent encoding and reconstruction of the intrinsic quasar spectra from the attenuated spectra and redshift (top). Then, it uses the reconstruction to mask absorption regions in the spectra for the next iteration (bottom). As additional absorption regions are masked with each iteration, SPENDERQ reconstructions converge to the intrinsic quasar spectra.

2. SPENDERQ

SPENDERQ uses the SPENDER autoencoder within an iterative framework for improving the fidelity of the intrinsic quasar spectrum reconstruction. We use SPENDER to learn a compact and redshift-invariant encoding of the intrinsic quasar spectra from the observed attenuated spectra and redshift. We use the same architecture as described in Melchior et al. (2023) with a 10-dimensional latent space² and a rest-frame model that spans the wavelength $\lambda = 800 - 3170 \text{ \AA}$ with 9,780 spectral elements.

The foreground IGM does not correlate with the background quasars, which means that the absorption features in the spectra do not correlate with the intrinsic quasar spectra³. In principle, this implies that SPENDER will not learn the absorption features since the absorptions are effectively random artifacts in the spectra. However, SPENDER, on its own, will learn the average *observed* spectrum, including absorption, and therefore underestimate the overall quasar continuum because absorption, treated as random noise, is neither additive nor does it have a mean of zero. To account for this effect, we combine SPENDER with an iterative procedure for identifying spectral elements with noticeable absorption.

At every iteration, we first train SPENDER using the conventional fidelity loss as well as similarity and consistency loss, as in Liang et al. (2023b). The similarity and consistency loss preserves locality

² We find no significant difference in performance among models with latent space dimensions of 6 to 12.

³ The total overall forest absorption correlates with redshift and, thus, the quasar; however, a specific absorption feature does not.

in the autoencoding process and leads to a redshift-invariant and nondegenerate latent-space distribution. Afterward, we coarsely rebin the quasar spectra, $f_q(\lambda)$, and the corresponding SPENDER reconstructions, $\tilde{f}_q(\lambda)$. The rebinning is done onto a wavelength grid, where the resolution, $\Delta\lambda$, is set by the median SNR per pixel of the spectrum at $\lambda < 1216 \text{ \AA}$ to $\Delta\lambda = 8/\text{SNR} \text{ \AA}$, with a minimum $\Delta\lambda > 4 \text{ \AA}$. This rebinning is only to identify regions with absorption and does not modify the resolution of the training data or the reconstruction.

Then, we identify spectral elements where f_q lies significantly below \tilde{f}_q based on a threshold that depends on $\sigma_q(\lambda)$, the observed uncertainty: $f_q < \tilde{f}_q - c\sigma_q$. We choose c using a data-driven approach based on the distribution of $(\tilde{f}_q - f_q)/\sigma_q$, where we can detect the continuum (see Appendix A for further details). Over the three wavelength ranges $\lambda < 1026 \text{ \AA}$, $1026 < \lambda < 1216 \text{ \AA}$, and $\lambda > 1216 \text{ \AA}$ regions, we use thresholds of $c = 0.8, 1.1$, and 3 , respectively. We mask these spectral elements by setting their weights to zero so that they do not contribute to the fidelity loss of the next training epoch. We repeat the iterations until the reconstructed quasar spectra converge to an estimate of the intrinsic spectra $\tilde{C}_q(\lambda)$, which we find to occur after roughly four iterations.

For the final SPENDERQ model, we ensemble five independently trained SPENDERQ models. Ensembling multiple models improves the robustness of the final model (Lakshminarayanan et al. 2016; Alsing et al. 2019; Hahn et al. 2024). Furthermore, we can also use the different models to quantify uncertainties on the SPENDERQ reconstructions. We present a schematic illustration of the SPENDERQ approach and architecture in Figure 1.

3. DESI YEAR 1 MOCKS

In this work, we apply SPENDERQ to synthetic Ly α data (hereafter; DESI Y1 mocks) created to validate the DESI first-year Ly α forest BAO analysis (DESI Collaboration et al. 2024a,b). The data are from a realization of the Ly α CoLoRe mocks presented in Cuceu et al. (2024). First, the CoLoRe package⁴(Ramírez-Pérez et al. 2022) is used to generate a set of transmitted flux fraction skewers and positions of quasars associated to them, based on log-normal Gaussian random fields. Next, the skewers are post-processed using the Ly α CoLoRe package⁵ (Farr et al. 2020) to introduce small-scale corrections and redshift-space distortions. The Ly α CoLoRe package also generates a catalog of high column density systems (HCDs) correlated with the Ly α density field. Lastly, realistic DESI-like mock quasar spectra are constructed from the Ly α CoLoRe package outputs using the quickquasars script⁶ (Herrera-Alcantar et al. 2023) in the desisim package⁷.

A subset of mock quasars are randomly selected to closely match the characteristics of the DESI Year 1 Ly α sample in terms of: footprint, redshift-magnitude relation, and mean SNR per pixel over $\lambda/(1+z_q) = 1040 - 1205 \text{ \AA}$. Then, absorption features from astrophysical effects are incorporated into the transmitted flux fractions of the selected quasars. The mocks include astrophysical effects from HCDs, which are modeled using a Voigt profile. They also include Broad Absorption Lines (BALs), randomly introduced into 16% of the spectra based on a set of templates (Martini et al. 2024), and absorption features from other transition lines (metals), which are added by re-scaling the

⁴ <https://github.com/damonge/CoLoRe>

⁵ <https://github.com/igmhub/LyaCoLoRe>

⁶ <https://github.com/desihub/desisim/blob/main/py/desisim/scripts/quickquasars.py>

⁷ <https://github.com/desihub/desisim>

$\text{Ly}\alpha$ transmitted flux fraction according to each transition and shifting the absorption features to the appropriate wavelengths. For additional details, we refer readers to Section 2.3 of [Herrera-Alcantar et al. \(2025\)](#).

The transmitted flux fractions with all these features are then multiplied to unabsorbed quasar spectrum, which are templates assigned to the quasars based on r -band magnitude and redshift using the `SIMQSO` library⁸ ([McGreer et al. 2021](#)). Instrumental noise is then introduced into the quasar spectra using `specsims`⁹ ([Kirkby et al. 2016](#)), which emulates the DESI spectrograph and the nominal DESI dark-time program observational conditions. We refer the reader to [Ramírez-Pérez et al. \(2022\)](#); [Farr et al. \(2020\)](#); [Herrera-Alcantar et al. \(2023\)](#) and [Cuceu et al. \(2024\)](#) for further details on `CoLoRe`, `LyαCoLoRe`, `quickquasars`, and the DESI Y1 mocks, respectively.

For this work, we limit our analysis to quasar spectra with redshifts between the range $2.1 < z < 3.5$. The lower bound corresponds to the redshift limit of the DESI $\text{Ly}\alpha$ sample in [DESI Collaboration et al. \(2024c\)](#) and ensures that all of the quasars have some rest-frame wavelength overlap. The upper bound is the nominal limit for the DESI $\text{Ly}\alpha$ quasar tracers. Before applying SPENDERQ, we normalize the spectra to reduce their dynamical range. We divide them by the median spectral flux within $\lambda/(1+z_q) = 1600 - 1800\text{\AA}$. This range roughly corresponds to the wavelengths between the CIV and CIII emission lines, where there is little absorption overall from CIII. In total, our sample consists of 401,820 quasar spectra.

4. RESULTS

We present a comparison of the reconstructed intrinsic quasar spectra derived using SPENDERQ (red) to the DESI Y1 mock spectra (gray) in Figure 2. The spectra and reconstructions are plotted over the full observed-frame wavelength range in the left panels while the right panels focus on region A in the rest-frame ($\lambda/(1+z_q) = 1040 - 1205\text{\AA}$). All spectra are normalized (Section 3). We include the true intrinsic quasar continua (blue) and the spectra coarsely rebinned to 10\AA resolution (black), for comparison. For reference, we include the `picca` estimates of $\bar{F}(\lambda)C_q(\lambda)$ over regions A and “B” ($\lambda/(1+z_q) = 920 - 1020\text{\AA}$) in orange dashed. We also include the uncertainties of the SPENDERQ reconstructions by plotting the range of the predictions from all of the SPENDERQ models in the ensemble (shaded red). The quasars are randomly selected $z > 3$ quasars with higher signal-to-noise to showcase the full $\text{Ly}\alpha$ region and for clarity.

Overall, SPENDERQ accurately reconstructs the quasar spectra over the full observed wavelength range. This is especially clear redward of region A, $\lambda \gtrsim 1200\text{\AA}$, where absorption features are rarer. The broad emission lines of $\text{Ly}\beta$, $\text{Ly}\alpha$, SiIV, CIV, and CIII are well reconstructed and in excellent agreement with the true spectra in all of the selected quasars, even the asymmetric profiles of $\text{Ly}\alpha$ and $\text{Ly}\beta$. In region A, the SPENDERQ reconstructions successfully ignore absorption features and are in excellent agreement with the true quasar continua. We emphasize that SPENDERQ reconstructs the true quasar continua, C_q , unlike `picca`, which can only estimate $\bar{F}C_q$.

⁸ <https://github.com/imcgreer/simqso>

⁹ <https://github.com/desihub/specsim>

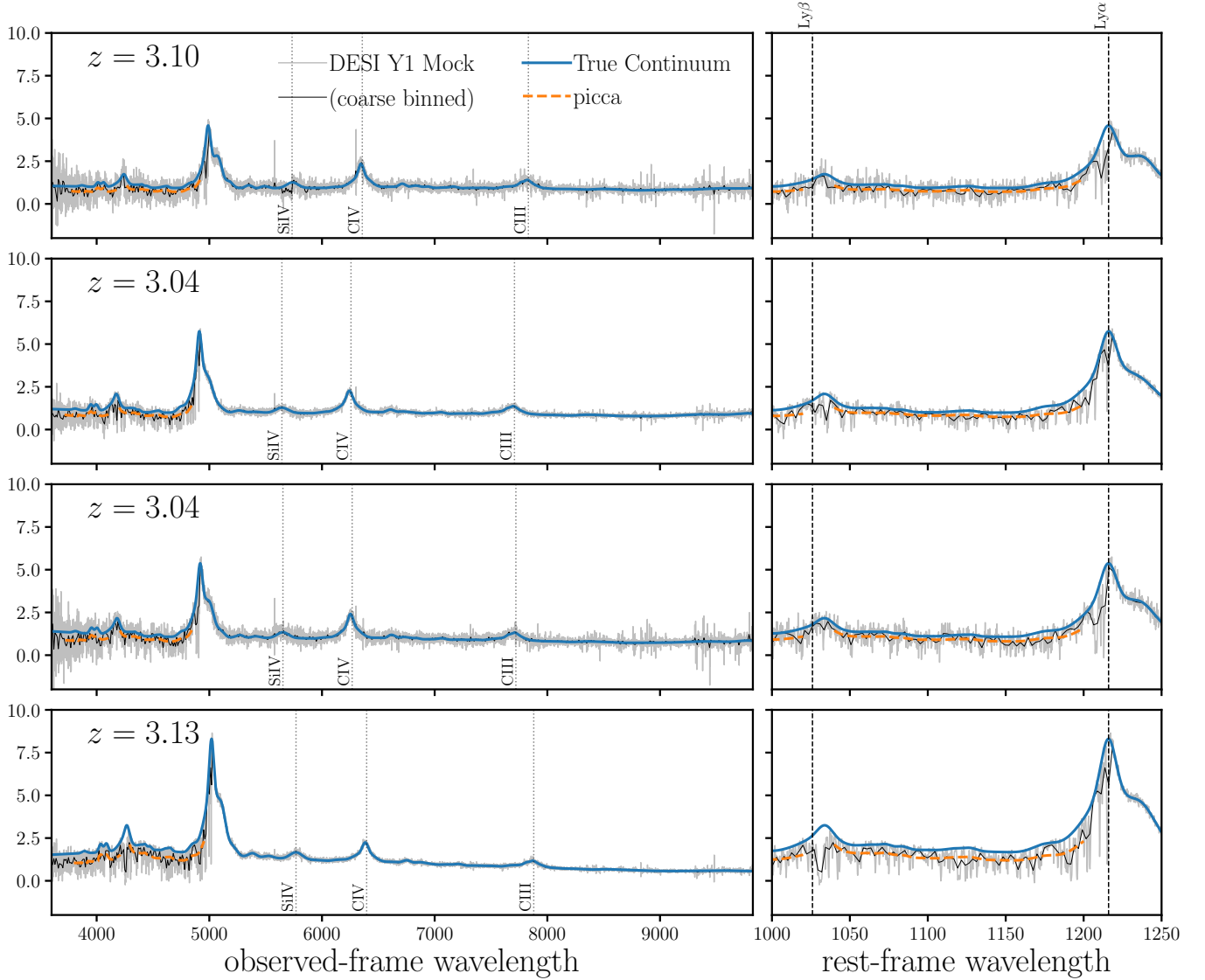


Figure 2. SPENDERQ reconstructed intrinsic quasar spectra (red) compared to the DESI Y1 mock spectra (gray). We plot randomly selected high redshift, $z > 3$, quasars with higher signal-to-noise to showcase the full $\text{Ly}\alpha$ region and for clarity. The left panels present the full spectra over the observed-frame wavelength. The right panels focus on region A in rest-frame wavelength. We include the true quasar spectra (blue), the coarsely rebinned spectra (black), and the `picca` $\overline{F}(\lambda)C_q(\lambda)$ estimates (orange dashed), for reference. SPENDERQ reconstructions are in excellent agreement with the true quasar spectra and, unlike `picca`, directly estimate the intrinsic quasar spectra, $C_q(\lambda)$.

In Figure 3, we present a quantitative assessment of SPENDERQ with the fractional residual of the reconstructions versus the true quasar spectra, $\tilde{f}_q/C_q - 1$ (blue), evaluated over all the mock spectra. The shaded region represents the 16 and 84th percentiles of the residuals. For reference, we mark the emission line wavelengths in black dashed. We also include the residuals of the `picca` $\overline{F}(\lambda)C_q(\lambda)$ estimates (orange) and the true $\overline{F}(\lambda)C_q(\lambda)$ (black dotted), for reference.

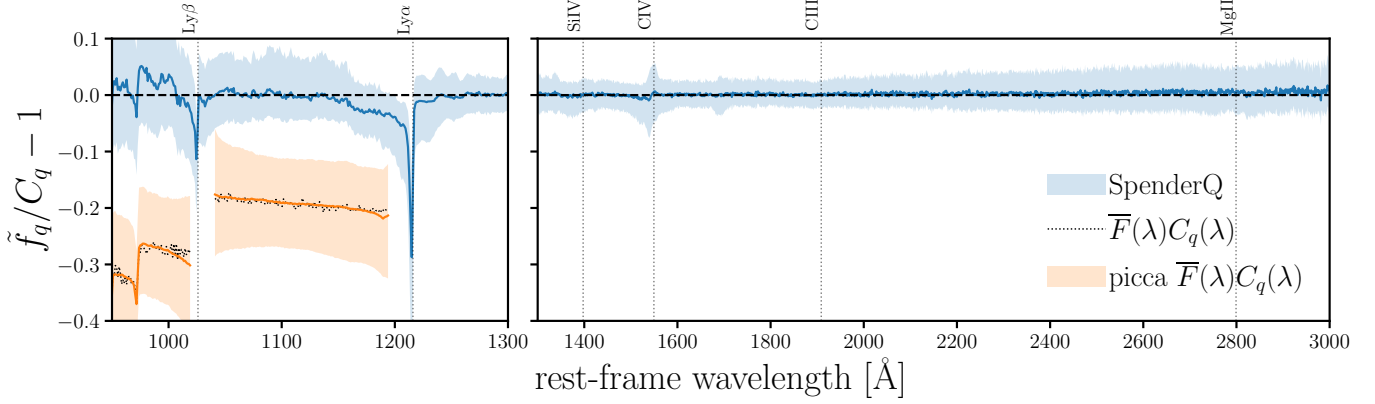


Figure 3. Fractional residual of the SPENDERQ reconstruction versus the true quasar spectra over a broad rest-frame wavelength range. The shaded region represents the 16 and 84th percentiles of the residuals. For reference, we include the residuals of the **picca** $\bar{F}(\lambda)C_q(\lambda)$ estimates (orange) and the true $\bar{F}(\lambda)C_q(\lambda)$ (black dotted). Redward of Ly α , SPENDERQ provides percent level reconstructions of the true spectra (right). Blueward of Ly α , SPENDERQ reproduces the true spectra with a mean residual of <5% (left).

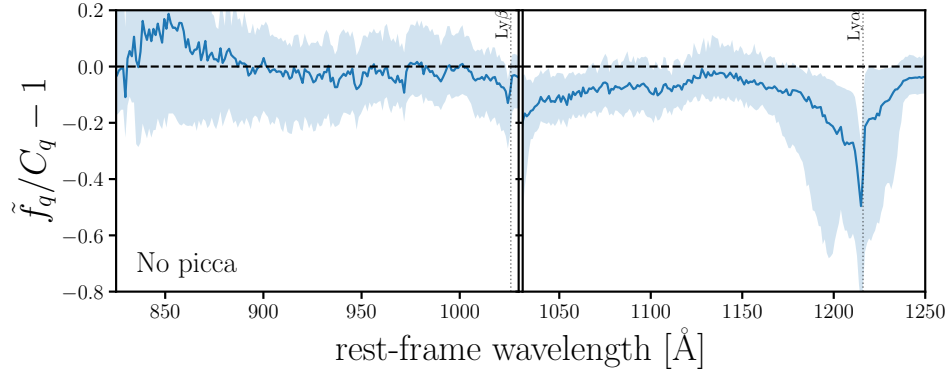


Figure 4. Fractional residual of the SPENDERQ reconstruction versus the true spectra for quasars with no **picca** reconstruction. **picca** fails to fit $\sim 5\%$ of the spectra for region A and $\sim 70\%$ of the spectra for region B where there are fewer than 150 spectral elements. The shaded region represents the 16 and 84th percentiles of the residuals. Even for spectra with no **picca** reconstructions, SPENDERQ produces reconstructions of the quasar spectra with $\lesssim 10\%$ residuals.

Redward of Ly α , $\lambda/(1+z_q) \gtrsim 1250\text{\AA}$, SPENDERQ reproduces the true spectra to percent level (right panel). We note that the performance of SPENDERQ is worse at longer wavelengths, $\lambda/(1+z_q) > 2800\text{\AA}$, with a slightly broader distribution of residuals. This is due to the fact that we normalize the spectra by the median flux within $\lambda/(1+z_q) = 1600 - 1800\text{\AA}$ (Section 3). Nevertheless, the residuals demonstrate that even without any additional postprocessing SPENDERQ is capable of accurately detecting and measuring SiIV, CIV, CIII, and MgII metal absorption lines that probe the gas content in the high redshift Universe.

In region A, SPENDERQ reproduces the true spectra with mean residual <5%. In fact, over $\lambda/(1+z_q) = 1040 - 1150\text{\AA}$, the mean SPENDERQ residual is <1%, with no noticeable wavelength

dependence. Although we refrain from direct comparison of the residuals with `picca`, as it estimates \overline{FC}_q and not C_q , we note that the SPENDERQ reconstructions are more precise. The shaded region is $1.5\times$ narrower than the shaded region of `picca`.

In region B, blueward of $\text{Ly}\beta$, $\lambda/(1+z_q) \lesssim 1050\text{\AA}$, SPENDERQ performs noticeably worse. This region is affected by both $\text{Ly}\alpha$, $\text{Ly}\beta$, and other Lyman series absorption and is only available in spectra of quasars with $z > 2.4$. Even for the $z > 2.4$ quasars, region B is at the edge of the DESI spectral range, with lower throughput, and thus is noisier (e.g., [Chaussidon et al. 2023](#)). Nevertheless, SPENDERQ reconstructions have mean residuals of $<5\%$ with similar precision as `picca`.

We note that SPENDERQ’s performance is despite the fact that we do not preprocess the spectra to mask BAL and damped $\text{Ly}\alpha$ (DLA) systems¹⁰. However, because we do not mask BALs there is a significant residual in the emission line regions of $\text{Ly}\alpha$ and $\text{Ly}\beta$. On the blue side of the lines, there is a $\sim 3\%$ suppression in the reconstructions. This is caused by the fact that absorption from BAL features can correlate with the intrinsic quasars and, thus, is learned by SPENDERQ. We discuss this further in Section 5.

In addition to directly estimating quasar continua, SPENDERQ also provides reconstructions for all spectra. `picca` does not fit a spectrum if it has less than 150 spectral elements in the wavelength range. This excludes $\sim 5\%$ of the spectra for region A and $\sim 70\%$ of the spectra for region B. However, SPENDERQ can reconstruct the quasar spectra for all quasars. In Figure 4, we present the SPENDERQ residuals for quasar spectra with no `picca` fits for region B (left) and no fits for region A (right). Despite the limited data, SPENDERQ produces reconstructions with residuals of $\sim 10\%$. SPENDERQ is able to do this because it leverages many correlated features throughout the entire spectra to produce accurate reconstructions (see also discussion in [Melchior et al. 2023](#)).

In Figure 5, we further examine SPENDERQ’s performance; this time for individual spectra. We present the fractional residuals of SPENDERQ reconstructions for a set of spectra randomly sampled across our redshift range (blue). For comparison, we include the residuals of the `picca` \overline{FC}_q estimates (orange), the true \overline{FC}_q (black dotted), and the observed spectrum (black). For some of the spectra the `picca` estimates have significantly biased slopes compared to the true \overline{FC}_q , blueward of $\text{Ly}\alpha$. This is particularly the case when region A or B falls near the edge of the DESI wavelength range with low signal-to-noise. Meanwhile, SPENDERQ accurately reconstructs the shape of the continua, even in the low signal-to-noise regimes.

To quantitatively access SPENDERQ’s performance on individual spectra, we calculate the absolute fractional flux error (AFFE; e.g., [Liu & Bordoloi 2021](#); [Turner et al. 2024](#)) of its reconstructions:

$$|\delta C_q| = \frac{\int_{\lambda_1}^{\lambda_2} \left| \frac{\tilde{f}_q(\lambda) - C_q(\lambda)}{C_q(\lambda)} \right| d\lambda}{\int_{\lambda_1}^{\lambda_2} d\lambda}. \quad (1)$$

We evaluate the AFFE over the $\text{Ly}\alpha$ region ($\lambda_1 = 1040$ and $\lambda_2 = 1200\text{\AA}$) for all mock spectra with `picca` reconstructions. In Figure 6, we present the distribution of the AFFE for SPENDERQ

¹⁰ This preprocessing is included in `picca`.

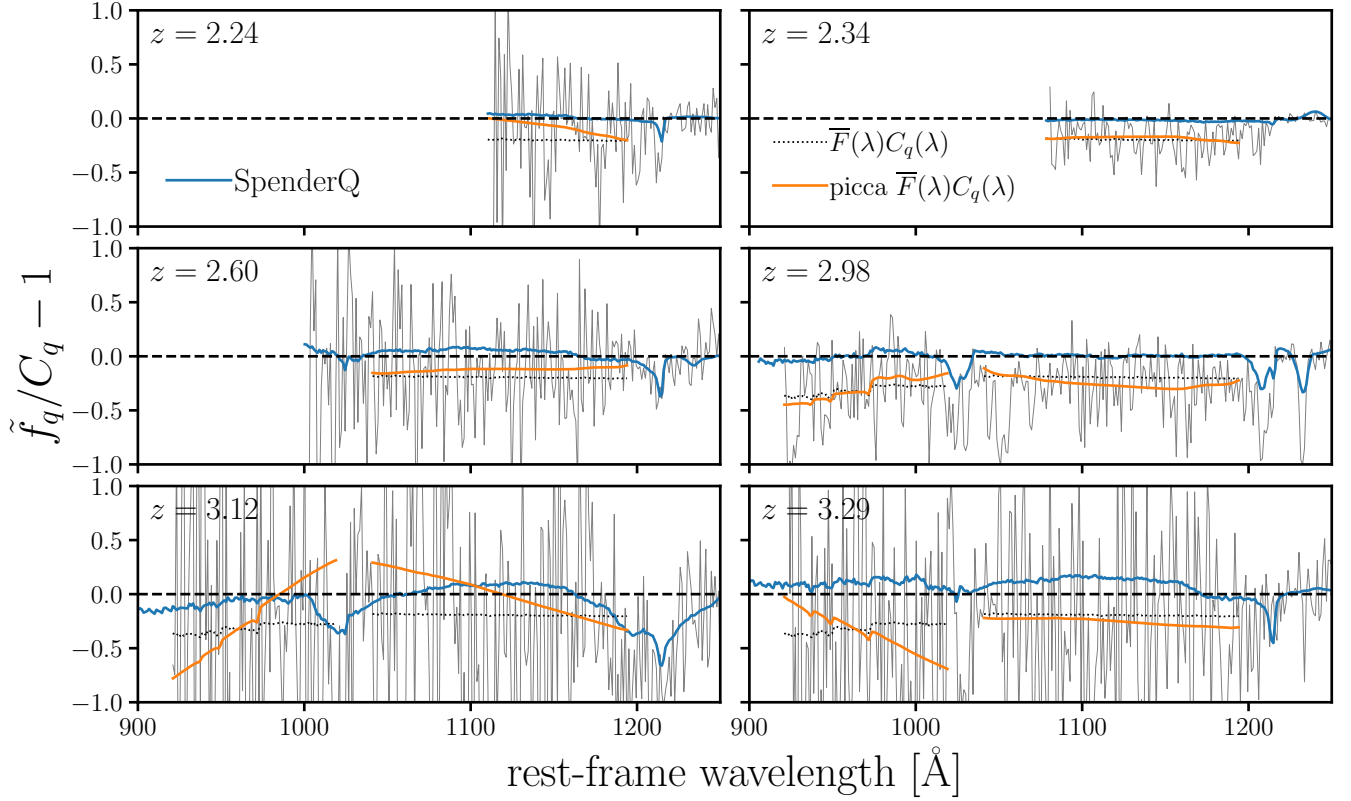


Figure 5. Fractional residual of the SPENDERQ reconstruction (blue) for individual spectra for random quasars across $2.1 < z < 3.5$. We include residuals of the `picca` $\bar{F}C_q$ estimates (orange), the true $\bar{F}C_q$, and the mock observed spectrum (black) for comparison. Even for a small sample of randomly selected quasars, the comparison reveals cases where `picca` dramatically misestimates the shape of $\bar{F}C_q$. Meanwhile, SPENDERQ provides more robust reconstructions that accurately capture the shape of the continuum.

reconstructions (blue). We also present the AFFE distribution for `picca` (orange), where we evaluate AFFE for $\bar{F}C_q$ rather than C_q for an apples-to-apples comparison. Overall, SPENDERQ reconstructions have significantly lower AFFE than `picca` with median AFFE of 0.04 versus 0.08. Furthermore, with SPENDERQ we have fewer reconstructions with large AFFE: e.g., less than 1.5% have AFFE > 0.2 compared to $\sim 10\%$ for `picca`. We also include in Figure 6 the SPENDERQ and `picca` AFFE distributions for spectra with lower SNR (solid lines). These spectra have median SNR per pixel < 1 and account for half of the spectra. The AFFE is higher for lower SNR spectra, for both SPENDERQ and `picca`. However, SPENDERQ has significantly lower AFFE even for lower SNR spectra. The comparisons in Figure 5 and 6 demonstrate: SPENDERQ reconstructions are not only accurate and more precise overall, but also more robust for individual spectra.

5. DISCUSSION

We demonstrate the advantages of SPENDERQ over the current state-of-the-art. SPENDERQ directly estimates the quasar continua, not $\bar{F}(\lambda)C_q(\lambda)$. Its reconstructions are overall unbiased and more precise. It also more accurately reconstructs individual quasar spectra and can be applied to all spectra, even ones with limited coverage of region A or B.

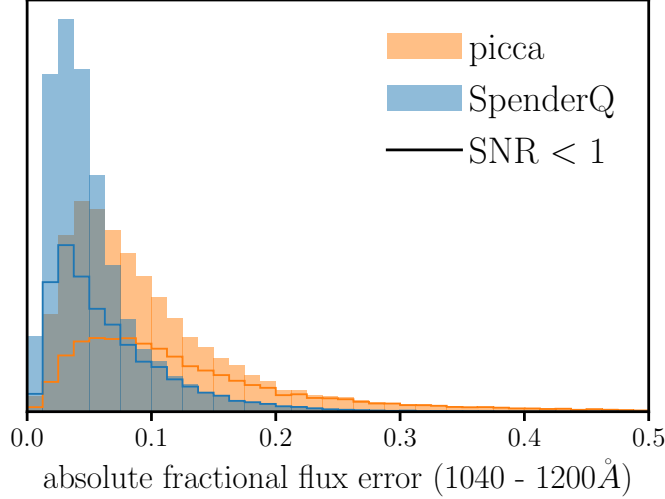


Figure 6. The distribution of absolute fractional flux error (AFFE) of the SPENDERQ (blue) and the `picca` reconstructions (orange). We calculate the AFFE for all mock spectra with `picca` reconstructions in region A and over the wavelength range: 1040 - 1200Å. For `picca`, we calculate AFFE with respect to $\overline{F}C_q$ as it estimates $\overline{F}C_q$, not C_q . We also include the AFFE distributions for spectra with low SNR < 1 (solid line). The comparison of the AFFE distributions illustrates that SPENDERQ provides more accurate and precise quasar continuum reconstructions.

Residuals in the quasar continuum bias flux transmission field derived from them. This in turn significantly distorts Ly α clustering measurements (Busca et al. 2013; Slosar et al. 2013; Delubac et al. 2015; Blomqvist et al. 2015; Bautista et al. 2017). For example, the amplitude and wavelength dependence of the residual suppress the monopole of power spectrum by a factor of two on large scales ($k < 0.1 h^{-1}\text{Mpc}$) and also distorts the shape of all the multipoles (de Belsunce et al. 2024). With SPENDERQ, we expect to significantly reduce this distortion and reduce the systematics in Ly α clustering analyses.

Despite the improvements, SPENDERQ does not accurately reconstruct every spectra. For 0.25% of the spectra, the median SPENDERQ fractional residual in the Ly α range exceed 25%. These spectra fall broadly under two categories. The first are spectra with low signal-to-noise. 99% of the spectra with higher residuals have SNR < 1 . The second are spectra with higher SNR but with major broad absorption features in the Ly α emission from BALs. In the standard Ly α cosmological pipeline, spectra with BAL and DLAs are identified, then masked or removed by preprocessing steps before any reconstruction¹¹. In this work, we opt to keep these contaminants to fully test the capabilities of SPENDERQ. BALs come from high-velocity outflows (Weymann et al. 1991) and correlate with the intrinsic properties of quasar. SPENDERQ, therefore, learns these correlated features from these spectra, which impact their reconstruction. We show a few examples of these spectra in Appendix B, Figure 9.

¹¹ We include this preprocessing for the `picca` reconstructions in Figure 3.

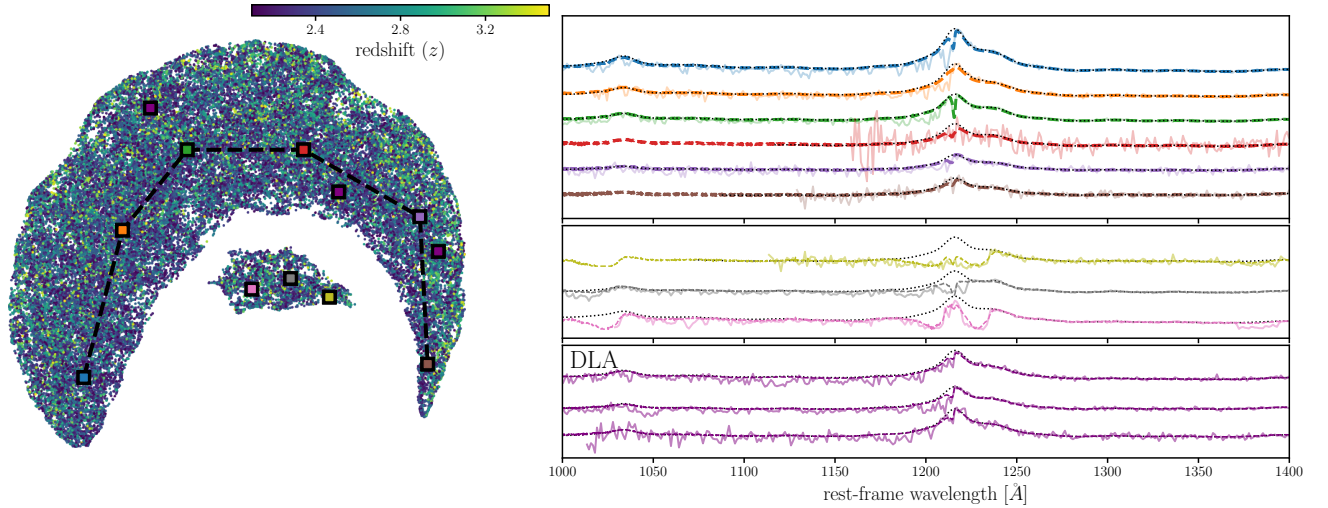


Figure 7. *Left:* The two-dimensional UMAP embedding of the SPENDERQ latent variables. We mark the redshifts of the quasars through the color bar. The embedding is split into two distinct groups. We find no significant redshift dependence in the embedding, which indicate that SPENDERQ learns a redshift invariant encoding of quasar spectra. *Right:* We examine the spectra of quasars marked in the UMAP embedding. The top and center panels present spectra from the upper and lower groups, respectively. The bottom panel presents spectra with DLAs. For reference, we include the true quasar spectra (black dotted) and the SPENDERQ reconstruction (dashed). The spectra are offset for clarity. The spectra in the upper panel show how the overall shape of quasar changes along the upper embedding. Meanwhile, the spectra in the lower embedding clearly show broad absorption features.

Fortunately for the spectra with BAL features, the latent variable space of SPENDERQ provides useful insights. In the left panel of Figure 7, we present the two-dimensional Uniform Manifold Approximation and Projection (UMAP; McInnes et al. 2018) embedding of the SPENDERQ latent variables. We color the quasars by their redshifts. The embedding reveals a clear separation of the quasars into two distinct clusters. In the right panels of Figure 7, we present the spectra for quasars marked in the UMAP embedding in the upper (top) and lower (center) clusters. We also present randomly selected spectra with DLAs (bottom). We offset the spectra for clarity and include the SPENDERQ reconstructions (dashed) and the true continuum (black dotted) for reference.

Each of the spectra in lower cluster display clear broad absorption features in the Ly α emission region. Indeed, we confirm that 99% of the spectra in this cluster have flagged BALs. This means we can use the SPENDERQ latent space to identify spectra with BALs and postprocess them to further improve their reconstruction. Alternatively, we can also apply SPENDERQ to the preprocessed dataset where spectra with BALs are masked or removed. This will only improve the performance of SPENDERQ. Meanwhile, the lower right panel illustrates that SPENDERQ reconstructions are robust to DLAs. Unlike BALs, DLAs do not correlate with the intrinsic quasar spectra so SPENDERQ reconstructions are not impacted by them.

The UMAP reveals additional insights into SPENDERQ. First, the color coding by redshift reveals that there is no significant redshift dependence throughout the latent space and confirms that SPENDERQ learns a redshift invariant encoding of the spectra. This further explains how SPENDERQ

produces better reconstructions in region B where `picca` struggles. It leverages higher redshift quasar spectra with better coverage for spectra with lower redshift quasars with little region B coverage. To further examine the latent space, we present the spectra of quasars along the marked track in the upper cluster in the top right panel of Figure 7. Quasars along this track have intrinsically different spectra with varying $\text{Ly}\alpha$ emission. This demonstrates that structure in the SPENDERQ latent space is physically informative and represent intrinsically different quasar spectra. Also, the SPENDERQ latent space can be used for outlier or anomaly detection as in Liang et al. (2023b,a); Böhm et al. (2023).

6. SUMMARY

We present SPENDERQ, a ML-based and fully data-driven method for reconstructing the intrinsic quasar spectra and measuring the $\text{Ly}\alpha$ forest. SPENDERQ leverages the SPENDER autoencoder to learn compact and redshift-invariant latent space representations of intrinsic quasar spectra. It combines this with an iterative procedure for identifying and masking absorption features to further improve the fidelity of the reconstructions. It relaxes any assumptions on the shape of the quasar continuum to produce unbiased $\text{Ly}\alpha$ forest measurements.

We apply SPENDERQ to synthetic quasar spectra used to validate the DESI first year $\text{Ly}\alpha$ forest BAO analysis and demonstrate its performance:

1. SPENDERQ accurately reconstructs the true intrinsic quasar spectra — not \overline{FC}_q — over the full wavelength range, including the broad emission lines ($\text{Ly}\beta$, $\text{Ly}\alpha$, SiIV, CIV, and CIII). For rest-frame $\lambda > 1215\text{\AA}$, SPENDERQ reconstructs the true continuum to percent level.
2. Over the $\text{Ly}\beta$ and $\text{Ly}\alpha$ ranges, the SPENDERQ reconstructions overall have $<5\%$ mean residuals compared to the true continuum. For region A, SPENDERQ is $1.5\times$ more precise than `picca`, the current state-of-the-art. This is despite not preprocessing the spectra to identify and mask BALs and DLAs, as done in standard $\text{Ly}\alpha$ clustering analyses.
3. Beyond its overall performance, SPENDERQ robustly reconstructs the shape of individual quasar spectra better than `picca`, with overall half the AFFE. It also reconstructs the continuum of all quasar spectra, even ones with limited data in regions A and B. With these improvements, SPENDERQ will significantly reduce the biases and distortions in $\text{Ly}\alpha$ clustering measurements.
4. SPENDERQ also provides latent variable encoding, or compression, of the quasar spectra that are redshift invariant and physically informative. This encoding can be used to identify interesting anomalies in the data. As a demonstration, we show that the encodings can be used to classify quasars with BAL.

In this work, we assess and benchmark SPENDERQ on mock spectra where we know the true intrinsic quasar spectra. We focus on how SPENDERQ significantly improves on the current state-of-the-art in recovering the quasar continuum. In subsequent works, we will again use the mocks to examine and quantify how the SPENDERQ improvements propagate to reducing distortions in

the Ly α forest clustering measurements and, then, the BAO and full-shape clustering cosmological analyses.

Furthermore, in an accompanying paper we apply SPENDERQ to DESI quasar spectra in the public Early Data Release (DESI Collaboration et al. 2024d,e). We present and publicly release the catalogs of the Ly α forest, metal absorbers, latent variables, and reconstructed quasar spectra all constructed using SPENDERQ. Furthermore, we present how SPENDERQ reconstructions can be used to study the physics of quasars. In subsequent works, we will use the latent variable catalog to identify outliers among the DESI quasars and also use the reconstructed quasar spectra to examine the variability of quasar spectra. We will also use the Ly α forest catalog for unbiased Ly α BAO and full-shape clustering cosmological analyses.

ACKNOWLEDGEMENTS

It’s a pleasure to thank Daniel Eisenstein, Julien Guy, Stephanie Juneau, and Paul Martini for useful discussions. This work was supported by the AI Accelerator program of the Schmidt Futures Foundation. This work was substantially performed using the Princeton Research Computing resources at Princeton University, which is a consortium of groups led by the Princeton Institute for Computational Science and Engineering (PICSciE) and Office of Information Technology’s Research Computing.

This research used data obtained with the Dark Energy Spectroscopic Instrument (DESI). DESI construction and operations is managed by the Lawrence Berkeley National Laboratory. This material is based upon work supported by the U.S. Department of Energy, Office of Science, Office of High-Energy Physics, under Contract No. DE-AC02-05CH11231, and by the National Energy Research Scientific Computing Center, a DOE Office of Science User Facility under the same contract. Additional support for DESI was provided by the U.S. National Science Foundation (NSF), Division of Astronomical Sciences under Contract No. AST-0950945 to the NSF’s National Optical-Infrared Astronomy Research Laboratory; the Science and Technology Facilities Council of the United Kingdom; the Gordon and Betty Moore Foundation; the Heising-Simons Foundation; the French Alternative Energies and Atomic Energy Commission (CEA); the National Council of Humanities, Science and Technology of Mexico (CONAHCYT); the Ministry of Science and Innovation of Spain (MICINN), and by the DESI Member Institutions: www.desi.lbl.gov/collaborating-institutions. The DESI collaboration is honored to be permitted to conduct scientific research on I’oligam Du’ag (Kitt Peak), a mountain with particular significance to the Tohono O’odham Nation. Any opinions, findings, and conclusions or recommendations expressed in this material are those of the author(s) and do not necessarily reflect the views of the U.S. National Science Foundation, the U.S. Department of Energy, or any of the listed funding agencies.

APPENDIX

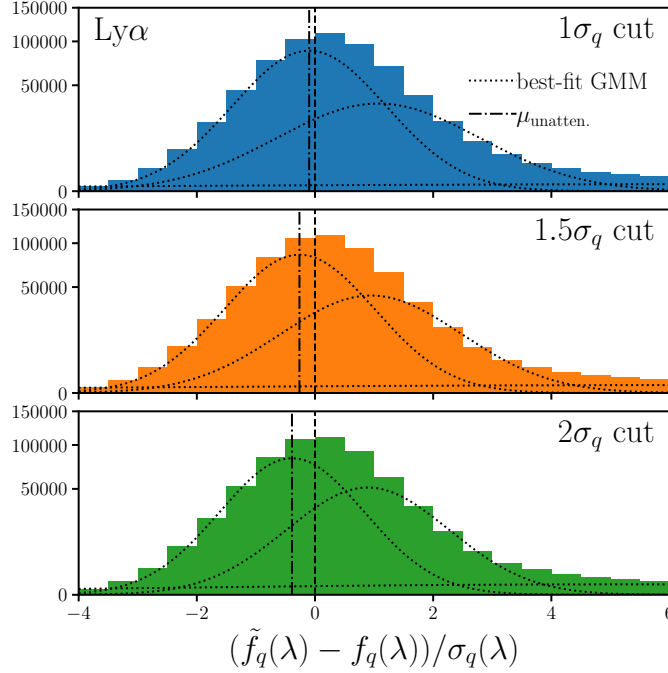


Figure 8. The distribution of residuals between the SPENDERQ reconstructions, \tilde{f}_q , and the observed spectra, f_q , normalized by observed uncertainty, σ_q . We mark the components of the best-fit GMM (dotted) and the mean of the component that corresponds to the unattenuated continuum (μ_{unatten} ; dot-dashed). We also include $(\tilde{f}_q - f_q)/\sigma_q = 0$ (dashed) for reference. The y-axis is scaled by the square function to clearly show all three GMM components. We use these distributions to determine the threshold used to identify the spectral elements

A. SPENDERQ ABSORPTION IDENTIFICATION

One key part of the SPENDERQ framework is using the SPENDER quasar continuum reconstructions, \tilde{f}_q , to identify and mask parts of the spectra with absorption for the next iteration. To do this, we compare \tilde{f}_q to f_q and identify the spectral elements where f_q lies below \tilde{f}_q by more than some threshold that depends on $\sigma_q(\lambda)$, the observed uncertainty: $f_q < \tilde{f}_q - c\sigma_q$. In principle, the threshold, c , should be set by the amount of absorption, with different values for different wavelength ranges (e.g. regions A and B). While c can be calibrated on simulations, we opt for a data-driven approach to make SPENDERQ independent from assumptions that go into simulations.

To determine the threshold, we first run SPENDERQ with different threshold values over a wide range, $c = 0.5 - 3$, until convergence. We then examine the distribution of $(\tilde{f}_q - f_q)/\sigma_q$, for the Ly β , Ly α , and $\lambda > 1215\text{\AA}$ wavelength ranges. Next, we fit Gaussian mixture models (GMM; McLachlan 2000) to the distributions. Then we identify the Gaussian component that correspond to the unattenuated continuum and select the c value where the unattenuated continuum component is centered most closely at 0.

In Figure 8, we show the distributions of $(\tilde{f}_q - f_q)/\sigma_q$ for the Ly α wavelength range for different thresholds: $c = 1$ (top), 1.5 (center), and 2 (bottom). The distributions have a consistent shape that is well-described by three Gaussian components. We mark the Gaussian components for the

distributions in each panel (black dotted) and include $(\tilde{f}_q - f_q)/\sigma_q = 0$ (dashed) for reference. One component, left-most, corresponds to the unattenuated continuum with $\sigma \approx 1$. The other two describe the attenuated spectral elements. We scale the y-axis by the square function to clearly show all three GMM components.

The mean corresponding to the unattenuated continuum component ($\mu_{\text{unatten.}}$; black dot-dashed) vary for the different thresholds. For the Ly α range, a threshold of $\sim 1\sigma_q$ results in the unattenuated continuum component to be centered at 0. This means that with this threshold, we accurately reconstruct the amplitude of the overall quasar continuum. We can use this approach because SPENDERQ reconstructions capture the intrinsic shape of the quasar continuum for individual spectra. This is demonstrated by the consistent shapes of the $(\tilde{f}_q - f_q)/\sigma_q$ distributions for different c .

B. SPENDERQ LIMITATIONS

Overall, SPENDERQ provides accurate reconstruction of individual quasar continua. However, for a small fraction of the spectra (0.25%) the median SPENDERQ fractional residual exceed 25% in the Ly α range. The vast majority (99.2%) of these are spectra with median SNR per pixel < 1 . The rest are spectra with higher SNR but with major broad absorption features in the Ly α emission from BALs. In Figure 9, we present examples of these spectra, i.e., four spectra with higher SNR > 0.25 . All of the spectra have BALs in their Ly α emission.

We further examine whether the SNR of the spectra impacts the latent encoding of SPENDERQ. In Figure 10, we present the two-dimensional UMAP embedding of the SPENDERQ latent variables, color-coded by the median SNR per pixel of the full spectra. Overall, we find little SNR dependence in the latent space. Interestingly, if we examine the SNR dependence together with the redshift dependence in the left panel of Figure 7, we find that the lower portion of the upper cluster is occupied by lower redshift quasars with lower SNR spectra. This suggests that there are fainter quasars at lower redshift that are not in the sample at higher redshifts. The SPENDERQ latent space suggests that they are intrinsically distinct from the higher redshift quasars in the sample.

REFERENCES

- | | |
|---|---|
| <p>Abdul Karim, M. L., Armengaud, E., Mention, G., et al. 2024, JCAP, 2024, 088,
doi: 10.1088/1475-7516/2024/05/088</p> <p>Ahumada, R., Allende Prieto, C., Almeida, A., et al. 2020, ApJS, 249, 3,
doi: 10.3847/1538-4365/ab929e</p> <p>Alsing, J., Charnock, T., Feeney, S., & Wandelt, B. 2019, Monthly Notices of the Royal Astronomical Society, 488, 4440,
doi: 10.1093/mnras/stz1960</p> <p>Bagherian, H., Joseph, M., Schmaltz, M., & Sivaraajan, E. N. 2024, arXiv e-prints, arXiv:2405.17554,
doi: 10.48550/arXiv.2405.17554</p> | <p>Bautista, J. E., Busca, N. G., Guy, J., et al. 2017, A&A, 603, A12,
doi: 10.1051/0004-6361/201730533</p> <p>Blomqvist, M., Kirkby, D., Bautista, J. E., et al. 2015, JCAP, 2015, 034,
doi: 10.1088/1475-7516/2015/11/034</p> <p>Böhm, V., Kim, A. G., & Juneau, S. 2023, MNRAS, 526, 3072,
doi: 10.1093/mnras/stad2773</p> <p>Busca, N. G., Delubac, T., Rich, J., et al. 2013, A&A, 552, A96,
doi: 10.1051/0004-6361/201220724</p> |
|---|---|

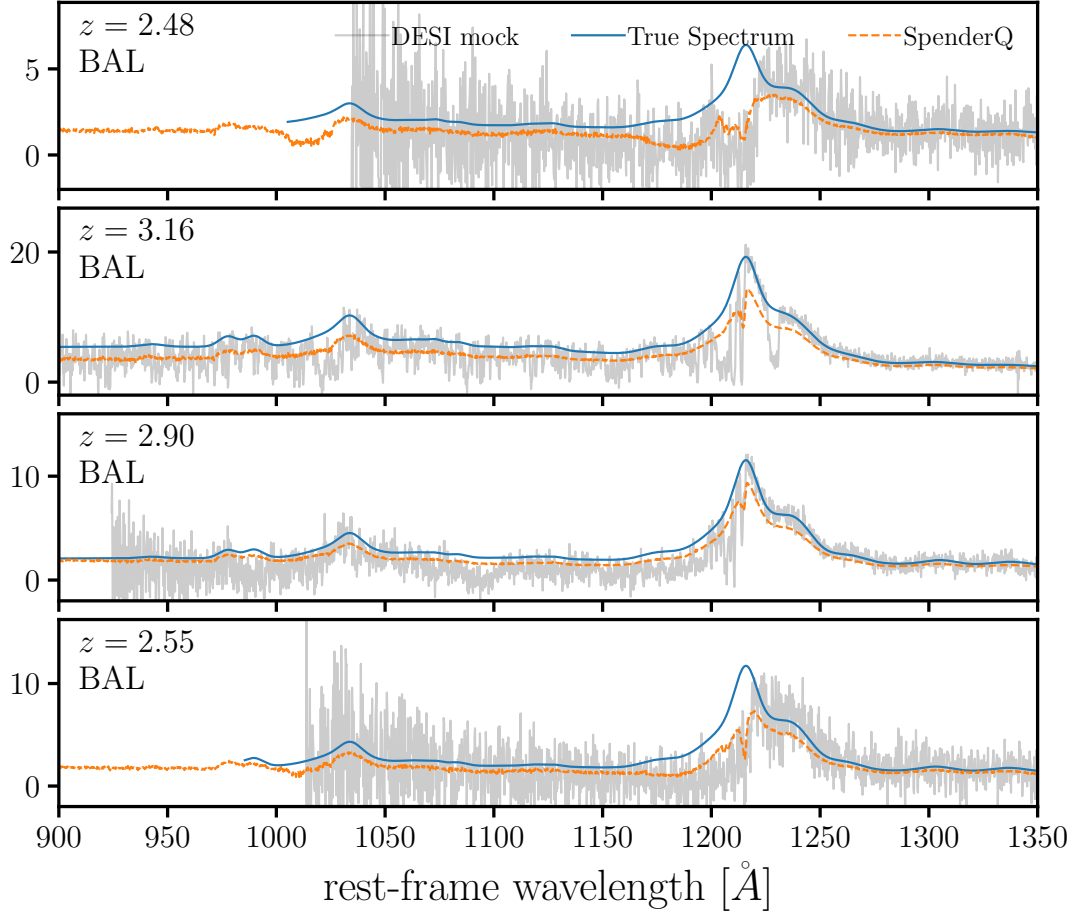


Figure 9. Higher signal-to-noise ($\text{SNR} > 0.25$) spectra where the median SPENDERQ residual in the $\text{Ly}\alpha$ range exceeds 25%. All of the spectra have broad absorption features in the $\text{Ly}\alpha$ emission from BAL. In the standard approach, spectra with these features are identified and removed in preprocessing steps before the reconstruction with `picca`. In SPENDERQ, we can either use the same preprocessing steps or these spectra can be identified in the latent space, as we show in Figure 7.

Chaussidon, E., Yèche, C., Palanque-Delabrouille, N., et al. 2023, *ApJ*, 944, 107,
doi: [10.3847/1538-4357/acb3c2](https://doi.org/10.3847/1538-4357/acb3c2)

Cuceu, A., et al. 2024.
<https://arxiv.org/abs/2404.03004>

Davies, F. B., Hennawi, J. F., Bañados, E., et al. 2018, *ApJ*, 864, 143,
doi: [10.3847/1538-4357/aad7f8](https://doi.org/10.3847/1538-4357/aad7f8)

de Belsunce, R., Philcox, O. H. E., Iršič, V., et al. 2024, *MNRAS*, 533, 3756,
doi: [10.1093/mnras/stae2035](https://doi.org/10.1093/mnras/stae2035)

Delubac, T., Bautista, J. E., Busca, N. G., et al. 2015, *A&A*, 574, A59,
doi: [10.1051/0004-6361/201423969](https://doi.org/10.1051/0004-6361/201423969)

DESI Collaboration, Aghamousa, A., Aguilar, J., et al. 2016a, arXiv:1611.00036 [astro-ph].

<https://arxiv.org/abs/1611.00036>
—. 2016b, arXiv:1611.00037 [astro-ph].
<https://arxiv.org/abs/1611.00037>

DESI Collaboration, Abaresi, B., Aguilar, J., et al. 2022, *AJ*, 164, 207,
doi: [10.3847/1538-3881/ac882b](https://doi.org/10.3847/1538-3881/ac882b)

DESI Collaboration, Adame, A. G., Aguilar, J., et al. 2024a, arXiv e-prints, arXiv:2404.03001,
doi: [10.48550/arXiv.2404.03001](https://doi.org/10.48550/arXiv.2404.03001)

DESI Collaboration, Adame, A. G., Aguilar, J., et al. 2024b, arXiv e-prints, arXiv:2404.03000,
doi: [10.48550/arXiv.2404.03000](https://doi.org/10.48550/arXiv.2404.03000)

—. 2024c, arXiv e-prints, arXiv:2404.03001,
doi: [10.48550/arXiv.2404.03001](https://doi.org/10.48550/arXiv.2404.03001)

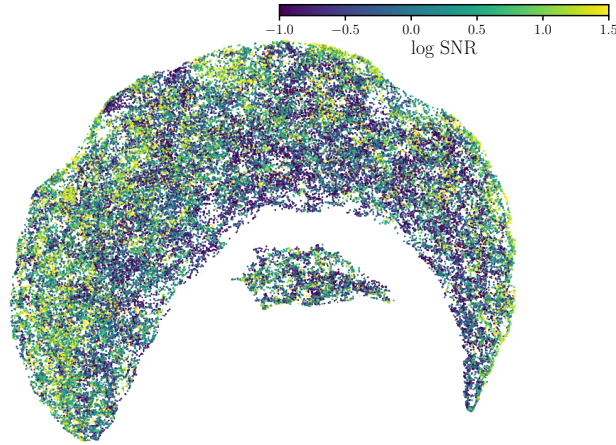


Figure 10. Two-dimensional UMAP embedding of the SPENDERQ latent variables color coded by SNR. The SNR represent the median SNR per spectral element over the full wavelength range. Overall, we find no significant dependence of the latent space with SNR.

- . 2024d, *AJ*, 167, 62,
doi: [10.3847/1538-3881/ad0b08](https://doi.org/10.3847/1538-3881/ad0b08)
- . 2024e, *AJ*, 168, 58,
doi: [10.3847/1538-3881/ad3217](https://doi.org/10.3847/1538-3881/ad3217)
- du Mas des Bourboux, H., Rich, J., Font-Ribera, A., et al. 2020, *ApJ*, 901, 153,
doi: [10.3847/1538-4357/abb085](https://doi.org/10.3847/1538-4357/abb085)
- Eisenstein, D. J., Weinberg, D. H., Agol, E., et al. 2011, *The Astronomical Journal*, 142, 72,
doi: [10.1088/0004-6256/142/3/72](https://doi.org/10.1088/0004-6256/142/3/72)
- Farr, J., Font-Ribera, A., Bourboux, H. d. M. d., et al. 2020, *Journal of Cosmology and Astroparticle Physics*, 2020, 068–068,
doi: [10.1088/1475-7516/2020/03/068](https://doi.org/10.1088/1475-7516/2020/03/068)
- Faucher-Giguère, C.-A. 2020, *MNRAS*, 493, 1614,
doi: [10.1093/mnras/staa302](https://doi.org/10.1093/mnras/staa302)
- Font-Ribera, A., McDonald, P., Mostek, N., et al. 2014, *Journal of Cosmology and Astro-Particle Physics*, 05, 023,
doi: [10.1088/1475-7516/2014/05/023](https://doi.org/10.1088/1475-7516/2014/05/023)
- Guy, J., Bailey, S., Kremin, A., et al. 2023, *AJ*, 165, 144, doi: [10.3847/1538-3881/acb212](https://doi.org/10.3847/1538-3881/acb212)
- Haardt, F., & Madau, P. 2012, *ApJ*, 746, 125,
doi: [10.1088/0004-637X/746/2/125](https://doi.org/10.1088/0004-637X/746/2/125)
- Hahn, C., Eickenberg, M., Ho, S., et al. 2024, *PhRvD*, 109, 083534,
doi: [10.1103/PhysRevD.109.083534](https://doi.org/10.1103/PhysRevD.109.083534)
- Herrera-Alcantar, H. K., et al. 2023.
<https://arxiv.org/abs/2401.00303>
- Herrera-Alcantar, H. K., Muñoz-Gutiérrez, A., Tan, T., et al. 2025, *JCAP*, 2025, 141,
doi: [10.1088/1475-7516/2025/01/141](https://doi.org/10.1088/1475-7516/2025/01/141)
- Iršič, V., Viel, M., Haehnelt, M. G., et al. 2024, *PhRvD*, 109, 043511,
doi: [10.1103/PhysRevD.109.043511](https://doi.org/10.1103/PhysRevD.109.043511)
- Karaçaylı, N. G., Font-Ribera, A., & Padmanabhan, N. 2020, *MNRAS*, 497, 4742,
doi: [10.1093/mnras/staa2331](https://doi.org/10.1093/mnras/staa2331)
- Karaçaylı, N. G., Padmanabhan, N., Font-Ribera, A., et al. 2022, *MNRAS*, 509, 2842,
doi: [10.1093/mnras/stab3201](https://doi.org/10.1093/mnras/stab3201)
- Karaçaylı, N. G., Martini, P., Guy, J., et al. 2024, *MNRAS*, 528, 3941, doi: [10.1093/mnras/stae171](https://doi.org/10.1093/mnras/stae171)
- Kirkby, D., Bailey, S., Guy, J., & Weaver, B. A. 2016, Quick simulations of fiber spectrograph response v0.5, v0.5, Zenodo,
doi: [10.5281/zenodo.154130](https://doi.org/10.5281/zenodo.154130)
- Lakshminarayanan, B., Pritzel, A., & Blundell, C. 2016, arXiv e-prints, arXiv:1612.01474,
doi: [10.48550/arXiv.1612.01474](https://doi.org/10.48550/arXiv.1612.01474)
- Lee, K.-G., Suzuki, N., & Spergel, D. N. 2012, *AJ*, 143, 51, doi: [10.1088/0004-6256/143/2/51](https://doi.org/10.1088/0004-6256/143/2/51)
- Levi, M., Bebek, C., Beers, T., et al. 2013, arXiv e-prints, arXiv:1308.0847.
<https://arxiv.org/abs/1308.0847>
- Liang, Y., Melchior, P., Hahn, C., et al. 2023a, *The Astrophysical Journal*, 956, L6,
doi: [10.3847/2041-8213/acfa03](https://doi.org/10.3847/2041-8213/acfa03)
- Liang, Y., Melchior, P., Lu, S., Goulding, A., & Ward, C. 2023b, *The Astronomical Journal*, 166, 75, doi: [10.3847/1538-3881/ace100](https://doi.org/10.3847/1538-3881/ace100)
- Liu, B., & Bordoloi, R. 2021, *MNRAS*, 502, 3510,
doi: [10.1093/mnras/stab177](https://doi.org/10.1093/mnras/stab177)

- Madau, P., & Haardt, F. 2015, *ApJL*, 813, L8,
doi: [10.1088/2041-8205/813/1/L8](https://doi.org/10.1088/2041-8205/813/1/L8)
- Martini, P., et al. 2024.
<https://arxiv.org/abs/2405.09737>
- McGreer, I., Moustakas, J., & Schindler, J. 2021,
simqso: Simulated quasar spectra generator,
Astrophysics Source Code Library, record
ascl:2106.008. <http://ascl.net/2106.008>
- McInnes, L., Healy, J., & Melville, J. 2018,
UMAP: Uniform Manifold Approximation and
Projection for Dimension Reduction,
doi: [10.48550/arXiv.1802.03426](https://doi.org/10.48550/arXiv.1802.03426)
- McLachlan, G. 2000, A wiley-interscience
publication
- Melchior, P., Liang, Y., Hahn, C., & Goulding, A.
2023, *AJ*, 166, 74, doi: [10.3847/1538-3881/ace0ff](https://doi.org/10.3847/1538-3881/ace0ff)
- Miller, T. N., Doel, P., Gutierrez, G., et al. 2024,
AJ, 168, 95, doi: [10.3847/1538-3881/ad45fe](https://doi.org/10.3847/1538-3881/ad45fe)
- Pâris, I., Petitjean, P., Rollinde, E., et al. 2011,
A&A, 530, A50,
doi: [10.1051/0004-6361/201016233](https://doi.org/10.1051/0004-6361/201016233)
- Poppett, C., Tyas, L., Aguilar, J., et al. 2024, *AJ*,
168, 245, doi: [10.3847/1538-3881/ad76a4](https://doi.org/10.3847/1538-3881/ad76a4)
- Ramírez-Pérez, C., Sanchez, J., Alonso, D., &
Font-Ribera, A. 2022, *Journal of Cosmology and
Astroparticle Physics*, 2022, 002,
doi: [10.1088/1475-7516/2022/05/002](https://doi.org/10.1088/1475-7516/2022/05/002)
- Ravoux, C., Abdul Karim, M. L., Armengaud, E.,
et al. 2023, *MNRAS*, 526, 5118,
doi: [10.1093/mnras/stad3008](https://doi.org/10.1093/mnras/stad3008)
- Robertson, B. E., Ellis, R. S., Furlanetto, S. R., &
Dunlop, J. S. 2015, *ApJL*, 802, L19,
doi: [10.1088/2041-8205/802/2/L19](https://doi.org/10.1088/2041-8205/802/2/L19)
- Schlafly, E. F., Kirkby, D., Schlegel, D. J., et al.
2023, *AJ*, 166, 259,
doi: [10.3847/1538-3881/ad0832](https://doi.org/10.3847/1538-3881/ad0832)
- Silber, J. H., Fagrelus, P., Fanning, K., et al.
2023, *AJ*, 165, 9, doi: [10.3847/1538-3881/ac9ab1](https://doi.org/10.3847/1538-3881/ac9ab1)
- Slosar, A., Iršič, V., Kirkby, D., et al. 2013, *JCAP*,
2013, 026, doi: [10.1088/1475-7516/2013/04/026](https://doi.org/10.1088/1475-7516/2013/04/026)
- Sun, Z., Ting, Y.-S., & Cai, Z. 2023, *ApJS*, 269, 4,
doi: [10.3847/1538-4365/acf2f1](https://doi.org/10.3847/1538-4365/acf2f1)
- Suzuki, N., Tytler, D., Kirkman, D., O'Meara,
J. M., & Lubin, D. 2005, *ApJ*, 618, 592,
doi: [10.1086/426062](https://doi.org/10.1086/426062)
- Turner, W., Martini, P., Karaçaylı, N. G., et al.
2024, *ApJ*, 976, 143,
doi: [10.3847/1538-4357/ad8239](https://doi.org/10.3847/1538-4357/ad8239)
- Weymann, R. J., Morris, S. L., Foltz, C. B., &
Hewett, P. C. 1991, *ApJ*, 373, 23,
doi: [10.1086/170020](https://doi.org/10.1086/170020)